

SAM Code Validation using the Compact Integral Effects Test (CIET) Experimental Data

Nuclear Science & Engineering Division

About Argonne National Laboratory

Argonne is a U.S. Department of Energy laboratory managed by UChicago Argonne, LLC under contract DE-AC02-06CH11357. The Laboratory's main facility is outside Chicago, at 9700 South Cass Avenue, Argonne, Illinois 60439. For information about Argonne and its pioneering science and technology programs, see www.anl.gov.

DOCUMENT AVAILABILITY

Online Access: U.S. Department of Energy (DOE) reports produced after 1991 and a growing number of pre-1991 documents are available free at OSTI.GOV (<http://www.osti.gov/>), a service of the U.S. Dept. of Energy's Office of Scientific and Technical Information

Reports not in digital format may be purchased by the public from the National Technical Information Service (NTIS):

U.S. Department of Commerce
National Technical Information Service
5301 Shawnee Rd
Alexandria, VA 22312
www.ntis.gov
Phone: (800) 553-NTIS (6847) or (703) 605-6000
Fax: (703) 605-6900
Email: **orders@ntis.gov**

Reports not in digital format are available to DOE and DOE contractors from the Office of Scientific and Technical Information (OSTI):

U.S. Department of Energy
Office of Scientific and Technical Information
P.O. Box 62
Oak Ridge, TN 37831-0062
www.osti.gov
Phone: (865) 576-8401
Fax: (865) 576-5728
Email: **reports@osti.gov**

Disclaimer

This report was prepared as an account of work sponsored by an agency of the United States Government. Neither the United States Government nor any agency thereof, nor UChicago Argonne, LLC, nor any of their employees or officers, makes any warranty, express or implied, or assumes any legal liability or responsibility for the accuracy, completeness, or usefulness of any information, apparatus, product, or process disclosed, or represents that its use would not infringe privately owned rights. Reference herein to any specific commercial product, process, or service by trade name, trademark, manufacturer, or otherwise, does not necessarily constitute or imply its endorsement, recommendation, or favoring by the United States Government or any agency thereof. The views and opinions of document authors expressed herein do not necessarily state or reflect those of the United States Government or any agency thereof, Argonne National Laboratory, or UChicago Argonne, LLC.

SAM Code Validation using the Compact Integral Effects Test (CIET) Experimental Data

prepared by
Ling Zou, Rui Hu, and Anne Charpentier

Nuclear Science & Engineering Division
Argonne National Laboratory

June 2019

ABSTRACT

The primary objective of this study is to validate the system analysis code, SAM, using experimental data from the Compact Integral Effects Test (CIET) facility. The System Analysis Module (SAM) is an advanced and modern system analysis tool being developed at Argonne National Laboratory under the U.S. DOE Office of Nuclear Energy's Nuclear Energy Advanced Modeling and Simulation (NEAMS) program. Originally aiming at supporting sodium fast reactor (SFR) design, it is now extended to cover other non-light water reactor (non-LWR) concepts, such as high-temperature gas-cooled reactor (HTGR) designs, molten salt-fueled, and molten salt-cooled reactor designs. To support SAM code development for the wide range of non-LWR applications, it is of paramount importance to validate the code against experiments relevant to these reactor concepts. The Compact Integral Effects Test (CIET) facility, which was designed to reproduce the thermal-hydraulics response of fluoride salt-cooled high-temperature reactors (FHR) under both forced- and natural-circulation conditions, has been identified and selected as one of benchmark test facilities for SAM code validation. Among available CIET experiments, three sets of them with distinctive characteristics were selected for SAM code validation purpose. The three sets experiments are: 1) Power step change transient tests; 2) DHX-DRACS natural circulation tests; and 3) heater frequency response tests. For all tests, steady-state or transient, SAM-predicted results show very good agreement with experimental data. The successful validation of SAM against these selected CIET experiments demonstrates that the computer code is well suited for thermal-hydraulics analysis of FHR designs.

Contents

ABSTRACT	ii
Contents	iii
List of Figures	iv
List of Tables	iv
1 Introduction	1
2 CIET Experiment Setup	1
2.1 Identified Experiments for Validation	2
2.1.1 Power step change transient test	2
2.1.2 DHX-DRACS natural circulation test	3
2.1.3 Frequency response test	3
3 Validation	3
3.1 Modeling CIET Facility with SAM	3
3.1.1 Some details of the input model	4
3.2 Power step change transient test	6
3.3 DRACS/DHX Natural Circulation Tests	7
3.3.1 Isolated DRACS natural circulation test	8
3.3.2 Coupled DRACS-DHX natural circulation test	13
3.3.3 Frequency domain test	14
4 Conclusions and Discussions	18
ACKNOWLEDGEMENTS	19
REFERENCES	20
Appendices	21
Appendix A CIET Input Model	21
Appendix B Material Properties	25
B.1 304L stainless steel	25
B.2 Copper	25
B.3 Fiberglass	25
B.4 Dowtherm A	26
Appendix C Analytical Solutions for Isolated DRACS Natural Circulation	28

List of Figures

2.1	Schematic drawing of the CIET test facility (with permission to use from University of California, Berkeley).	2
3.1	The SAM input model for CIET facility	4
3.2	Power step change experiments, SAM simulation results compared with CIET experimental data. (SAM)=SAM simulation, (EXP)=Experiment.	7
3.3	SAM input model for the isolated DRACS loop.	8
3.4	Isolated DRACS natural circulation, SAM and RELAP5-3D simulation results compared with CIET experimental data. Top-left: $T_{TCHX,out}=46^{\circ}\text{C}$; Top-right: $T_{TCHX,out}=35^{\circ}\text{C}$; Bottom: $T_{TCHX,out}=40^{\circ}\text{C}$.	11
3.5	Isolated DRACS natural circulation, SAM simulation results compared with CIET experimental data	12
3.6	SAM input model for coupled DRACS-DHX natural circulations.	12
3.7	Coupled DRACS-DHX natural circulation, SAM and RELAP5-3D simulation results compared with CIET experimental data. Top-left: $T_{TCHX,out}=46^{\circ}\text{C}$; Top-right: $T_{TCHX,out}=35^{\circ}\text{C}$; Bottom: $T_{TCHX,out}=40^{\circ}\text{C}$.	14
3.8	Comparison between SAM predicted results (bottom) and experimental data (top) for fluid temperature at heater outlet, with input power frequency at 6×10^{-3} Hz.	16
3.9	Comparison between SAM predicted results (bottom) and experimental data (top) for wall surface temperature at heater outlet, with input power frequency at 6×10^{-3} Hz.	16
3.10	SAM predicted phase shift, heater outlet temperature compared to input power, for different input power frequencies.	17
3.11	SAM predicted heater outlet temperature amplitudes compared with experimental data for different input power frequencies.	17
A.1	Form loss coefficients used in the SAM CIET input model	24
B.1	Dowtherm A thermal physical properties implemented in SAM and RELAP5-3D.	27
C.1	A simplified schematic drawing of the DRACS loop	28
C.2	Temperature and density profiles in the simplified DRACS loop (C.L. = cold leg; H.L. = hot leg).	29

List of Tables

3.1	Added heat in the heater section during power step change transient test, q''_{wall} is equivalent heat flux on heater outer surface	6
3.2	Heat addition in the DHX tube walls for isolated DRACS natural circulation simulations, q'''_{wall} is equivalent volumetric heat source	9
3.3	Solution verification: SAM-predicted results vs. 'analytical' solutions for the simplified DRACS natural circulation. SAM=SAM-predicted results; ANA=analytical solution.	10
3.4	Heat addition in the heater outer walls for coupled DRACS-DHX natural circulation simulations, q'''_{wall} is equivalent volumetric heat source	13
3.5	Frequencies used in SAM validation	15
A.1	Pipe components of SAM input model for the CIET test facility	23
B.1	Temperature-dependent thermal conductivity and heat capacity for 304L stainless steel (Zweibaum, 2015)	25
B.2	Temperature-dependent thermal conductivity and heat capacity for copper (Zweibaum, 2015)	25
B.3	Temperature-dependent thermal conductivity for fiberglass (Zweibaum, 2015)	26

1 Introduction

The System Analysis Module (SAM) is a modern system analysis code being developed at Argonne National Laboratory for advanced non-light water reactor (non-LWR) safety analysis (Hu, 2017). Currently sponsored by DOE's NEAMS program, SAM code development has attracted a wide range of interest from the advanced non-LWR community, including, for example, Kairos Power to adopt SAM as its safety analysis tool. Recently, U.S. Nuclear Regulatory Commission (U.S. NRC) also intends to include SAM as the system and core thermal-hydraulics analysis code for design basis events in advanced non-LWRs (U.S.NRC, 2019).

Code validation plays an essential role in the development and assessment of reactor safety analysis codes. Extensive code validations have been performed to support the development of existing system analysis codes, such as RELAP5 (Inc., 1990) and TRACE (U.S.NRC, 2008), in supporting light water reactor designs. As new advanced non-LWR concepts emerge, there are gaps to be filled in both experiments and analysis tools. The Compact Integral Effects Test (CIET) facility was designed to reproduce the thermal-hydraulics response of fluoride salt-cooled high-temperature reactors (FHR) under forced- and natural-circulation conditions (Zweibaum et al., 2016). As a modern system analysis code intended for non-LWR safety analysis, it is of paramount importance to validate SAM against experiments highly relevant to these advanced non-LWR designs. Therefore, CIET facility has been identified and selected as one of benchmark test facilities for SAM code validation.

The primary objective of this work is to validate the SAM code against CIET experiments. Among available CIET experiments, three sets of them with distinctive characteristics were selected for SAM code validation purpose, including forced-convection power step change transient tests, DRACS (Direct reactor auxiliary cooling system)-DHX(DRACS heat exchanger) natural circulation tests, and heater frequency response tests. The forced-convection power step change transient tests provide data to validate SAM code in areas such as fluid properties, pump behaviors, conjugate heat transfer, and thermal inertia of both fluid and solid. The natural circulation tests provide data to validate SAM code in areas such as fluid properties, wall friction coefficients, and wall heat transfer coefficients. The frequency response tests focus on the heater section, and they provides additional data to validate the code in areas such as fluid/solid properties, conjugate heat transfer. In section 2, brief descriptions of the CIET facility and experiments identified for SAM validation will be given. Validation results will be presented and discussed in section 3. Following that, conclusions and discussions are provided.

2 CIET Experiment Setup

The Compact Integral Effects Test (CIET) experimental loop is a test facility that is designed, built and operated at University of California, Berkeley, with the aim to reproduce the thermal-hydraulics response of fluoride salt-cooled high-temperature reactors under forced- and natural-circulation conditions (Zweibaum et al., 2016). It also aims to provides experimental data to validate best-estimate computer code in order to support their use in reactor safety and licensing analysis.

In this section, only brief descriptions of the CIET test facility are included for purpose of completeness, with the focus on experimental setup, procedures, and results that are closely related to this SAM validation effort. More details of the CIET test facility, its design and instrumentation, and experiments are available in a series of UCB reports and dissertations, including (Bickel et al., 2014; Upadhya, 2015; Zweibaum, 2015; Zweibaum et al., 2016) among many others. As shown in figure 2.1, the CIET test facility consists of a primary loop and a DRACS loop, replicating the primary and DRACS flow loops of the Mk1 PB-FHR design (Andreades et al., 2014, 2016). In the primary loop, an electrical heater is installed to simulate the reactor core (heat source), a fan-driven air-cooled heat exchanger to simulate the coiled-tube air heater (CTAH, heat sink), and a pump to drive the flow (momentum source). This heater-CTAH-pump sub-loop simulates the primary loop of the Mk1 PB-FHR design under normal operation conditions. Under such conditions, flow through the DHX branch is restricted via flow diode installed in the DHX branch, which provides high flow resistance for upward flow, while low flow resistance for downward flow in the DHX branch. A by-pass flow

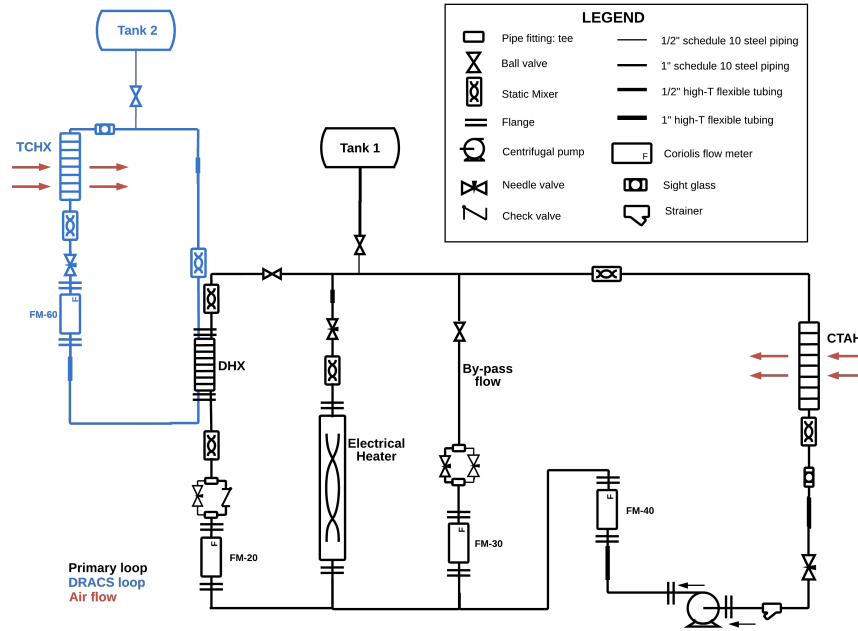


Figure 2.1: Schematic drawing of the CIET test facility (with permission to use from University of California, Berkeley).

branch is also installed in the facility, however, was not used in experiments related to SAM validation; and therefore, it is not included in SAM simulations discussed in later sections.

The scaled DRACS loop in the CIET test loop replicates such a loop in the Mk1 PB-FHR design, which provides passive decay heat removal capability during postulated accident scenarios, such as loss of forced convection (LOFT). In such transients, natural circulation is established in both the heater-DHX sub-loop and the DRACS loop, such that the heat is removed from the heater to DHX heat exchanger, and to TCHX, which is ultimately cooled by air.

2.1 Identified Experiments for Validation

Based on available experimental data and identified phenomena of interested on SAM validation, three sets of CIET experiments of distinctive characteristics have been identified to validate SAM computer code at this phase of validation effort.

2.1.1 Power step change transient test

In this test, experimental data were collected for transient, forced circulation conditions with heat input step changes in the electrical heater. The pump delivered a fixed coolant mass flow rate of 0.18 kg/s in the heater-CTAH-pump primary loop via automatic pump control. Both the by-pass and DHX branches were valve off and isolated from the primary flow loop. The CTAH outlet temperature was fixed at 80 °C also via automatically controlling its fan speed. Step change power inputs were applied to the electrical heater, and following each step change, the heater power was maintained as constant for about 600-1000 seconds, so stable conditions (flow rate and temperatures) could be reestablished in the loop. This experiment provides

valuable data to validate the SAM code in both conditions, e.g., quasi steady state when stable conditions were reestablished following each power step change, and transient system response during each power step change.

2.1.2 DHX-DRACS natural circulation test

The DHX-DRACS natural circulation test is dedicated to prove the passive decay heat removal concept of the Mk1 PB-FHR design during postulated accidents. Three sets of such tests have been selected for SAM validation. For each of these three tests, the TCHX outlet temperature is fixed at a given value by automatically varying the fan speed, while the heater power varied at different levels. Natural circulation flows are established in both the DHX and DRACS loops with different power inputs, and mass flow rates in both loops and coolant temperatures were measured. SAM is expected to predict correct natural circulation mass flow rates and oil temperature distributions in both loops.

2.1.3 Frequency response test

The frequency response test focuses on the primary loop, and more specifically on the heater section, under forced circulation conditions. The pump delivers a constant mass flow rate of 0.18kg/s in the primary loop. The CTAH outlet temperature is fixed at 80 °C, although in reality it fluctuates around that temperature. The heater has a sinusoidal input signal and the experiment measures the oil temperature as it exits the heater, as well as the surface temperature at the end of the heater. The frequency response test concerns in particular the phase shift and amplitude of the output signal compared to the input signal. The CIET experiment includes 11 different frequencies, among which 9 were usable to compare to SAM results. The two frequencies not compared were above 0.1 Hz, high limit of frequencies obtainable with the CIET.

3 Validation

In this section, SAM input model for the CIET facility as well as several details in modeling strategy will be first discussed. The following sections will be focused on validation results of the three selected sets of CIET experiments.

3.1 Modeling CIET Facility with SAM

This validation effort takes advantage of an existing one, i.e., validation of RELAP5-3D against CIET experiment ([Zweibaum, 2015](#)), which is a significant reference to build the SAM input model. Compared to the original RELAP5-3D input model, necessary modifications were made in the SAM input model, for example, when inconsistency in dimensions was found between the RELAP5-3D input model and their descriptions in corresponding document; and when SAM uses a different modeling strategy for certain components (e.g., Branch). Figure [3.1](#) shows the geometry and component naming of an initial SAM input model for the CIET test facility with the bypass branch excluded. More details of the input model are described in Appendix [A](#).

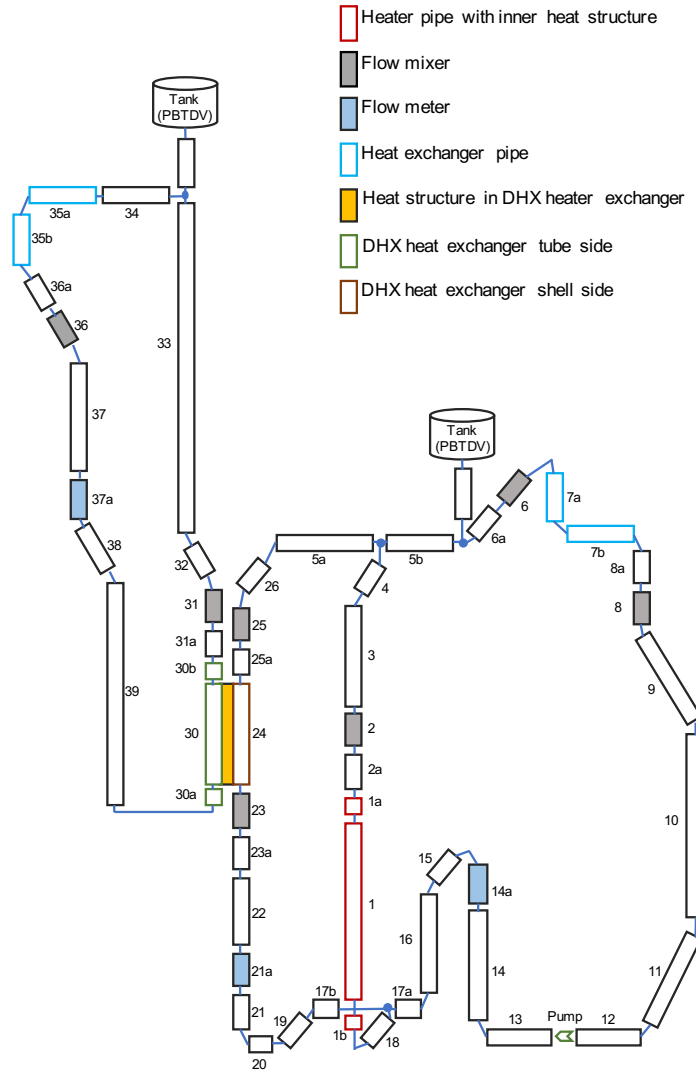


Figure 3.1: The SAM input model for CIET facility

3.1.1 Some details of the input model

For system analysis code, e.g., SAM, to simulate a real-life test facility, it is inevitable to introduce simplifications and approximations. Several modeling details are provided in this section on how and why certain components are modeled in SAM.

- Bypass branch:

The bypass branch is simply excluded in the SAM input model, as this branch was not used in any validation experiments.

- Pump:

In CIET experiment design, the pump uses a proportional controller to achieve the desired mass flow rate in the primary loop (Upadhyay, 2015). This feature was used in the power step change transient test to deliver a fixed mass flow rate in the primary loop. Currently, SAM's pump model is rather simplified

that it does not implement pump curves for pump simulation. Instead, the pump model allows users to input a pump head, and also allows for automatic pump head adjustment to match user-specified mass flow rate. In code validation, the pump model was able to deliver user-specified mass flow rate, as will be shown later.

- CTAH and TCHX:

In CIET experiment design, the CTAH in the primary loop and TCHX in the DRACS loop are identical oil-to-air fan-cooled heat exchangers. In most CIET experiments, the outlet temperatures of both heat exchangers are controlled to fixed values, which is achieved by automatically varying fan speed (Upadhy, 2015). In SAM simulations, both heat exchangers are simplified as pipe components. The desired outlet temperature is assigned as an artificial ambient temperature to pipe outer surface, and an arbitrary large heat transfer coefficient is assigned to the component outer surface, which forces its outlet temperature to be at the given artificial ambient temperature. A similar approach was also used in Zweibaum (2015).

In steady-state conditions, this strategy works very well to fix its outlet temperature at given values. In transient simulations, as it over-simplifies the heat transfer mechanism, the component's response to external perturbations, e.g., its inlet temperature change, is almost instantaneous. This is not true in experiments. The observed response time in CIET experiment, the time taken to re-establish a stable outlet temperature, is in the order of 100 seconds. Such a transient effect is not captured in SAM simulations, however, it is unimportant to this validation effort.

The arbitrary large heat transfer coefficient also makes the heat exchanger extremely effective in terms of utilizing its pipe length. As a consequence, in simulations, the coolant temperature almost instantaneously drops to the desired outlet temperature and stays unchanged along the pipe length. This introduces extra driven force in natural circulations, as the coolant in heat exchangers is colder, and thus 'heavier' than it should be in experiments. A slight modeling change is introduced to counter balance such an effect (discussed later).

- Static mixer and flowmeter:

In CIET experiment design, static mixers were made of nominal 1" diameter, schedule 40, 304L stainless steel piping containing internal mixing elements (Bickel et al., 2014). In SAM simulations, static mixers were modeled as bare schedule 10 pipes without internal mixing elements, and thus minor thermal inertial uncertainties are introduced. Note that this does not introduce friction loss uncertainty as the friction loss coefficient was originally fitted with schedule 10 pipe dimensions. This is also the reason to use schedule 10 pipe for static mixers, in order to better capture its friction loss. For the same reason, flowmeters are also modeled with schedule 10 pipes.

- Form losses:

For static mixer, flowmeter, and fan-cooled heat exchanger, due to their complexities in geometries, pressure loss coefficients are not readily available. In CIET experiments, combined pressure loss coefficients due to friction and form loss were provided for each of these three types of components. In a previous RELAP5-3D validation effort (Zweibaum, 2015), these correlations were tuned so model predicted natural circulation mass flow rate could match experiment data, which is believed not necessary in this validation effort. Instead, as discussed previously, a slight modeling change will be made in fan-cooled heat exchangers.

- Parasitic heat loss:

In CIET experiments, parasitic heat losses were significant in many cases, even with thermal insulation and guard heating. In the effort to validate RELAP5-3D, it was concluded that RELAP5-3D systematically underestimate parasitic heat losses in the primary loop by ~75% and in the DRACS loop by ~50%, likely due to additional losses through metallic components protruding from the thermal insulation Zweibaum (2015). This contributes to the largest uncertainty in both experiments and simulations.

In the RELAP5-3D model, heat transfer area densities were tuned to larger values to capture these additional losses. SAM sees similar trends and uses the same modeling strategy to compensate for such additional heat losses.

- Sight glass and flexible hoses

These items are simply not included and are replaced with same length schedule 10 pipes. This is believed to have minor effect to validation results as they only represent a trivial portion of the entire loop length.

3.2 Power step change transient test

This section describes SAM validation against the CIET power step change transient test. During the experiment, mass flow rate through the heater was controlled at 0.18 kg/s, and electric power applied to the heater followed step changes. Due to heat loss through heater out surface, heat added to coolant is smaller than the total electric power. In RELAP5-3D simulations, for each step change, added heat in the heater section is back calculated from heat balance when stabilized conditions were established, and they are listed as column 2 in Table 3.1. The same numbers are used and they are converted into equivalent heat flux on heater outer surface in SAM simulations.

Table 3.1: Added heat in the heater section during power step change transient test, q''_{wall} is equivalent heat flux on heater outer surface

Time [s]	Power [W]	q''_{wall} [W/m ²]
0	2512.9	11579.51
3244.77	2512.9	11579.51
3274.78	4218.7	19439.88
3935.16	4218.7	19439.88
3965.18	6072.5	27982.24
4590.54	6072.5	27982.24
4595.54	7085.2	32648.78
5292.73	7085.2	32648.78
5297.74	7598.2	35012.70
5953.08	7598.2	35012.70
5963.09	7156.4	32976.88
6784.00	7156.4	32976.88
6789.00	5435	25044.62
7439.33	5435	25044.62
7444.34	2710.1	12488.21
10000	2710.1	12488.21

SAM simulation results are plotted in Figure 3.2 along with experimental data. Overall, SAM simulation results agree quite well with experimental data. The bottom plot in Figure 3.2 shows the mass flow rate in both SAM simulation and experiment. The mass flow rate in experiment is slightly off from the specified value, 0.18 kg/s, while SAM simulation is able to maintain this flow rate. Nevertheless, the deviation is rather small, well within 1%, and only minor impact to experimental/numerical results is expected. From the top plot, when stable conditions are re-established following each power step change, SAM predicted temperatures show good agreement with experimental data. For the short time period following each power step change, the SAM model is able to capture the transient ramp up/down of heater outlet and CTAH outlet temperatures. This suggests that SAM models the thermal inertial of the flow loop pretty well. For the last two step changes in experiment, taking place at ~ 6784 and ~ 7439 second, the fan-cooled heat exchanger showed

obvious difficulty to quickly adjust its fan speed to get back to the fixed outlet temperature. This is reflected by the two large undershoot of CTAH outlet temperature following these two step changes. Consequently, such undershoot is also present in heater inlet/outlet and CTAH inlet temperatures. Such behaviors are not observed in SAM predicted temperatures. As discussed in section 3.1.1, SAM's CTAH components responses to external perturbation almost instantaneously. This can certainly be improved by implementing a more realistic control mechanism in SAM, however, it is beyond the scope of this validation effort, and is left for future studies.

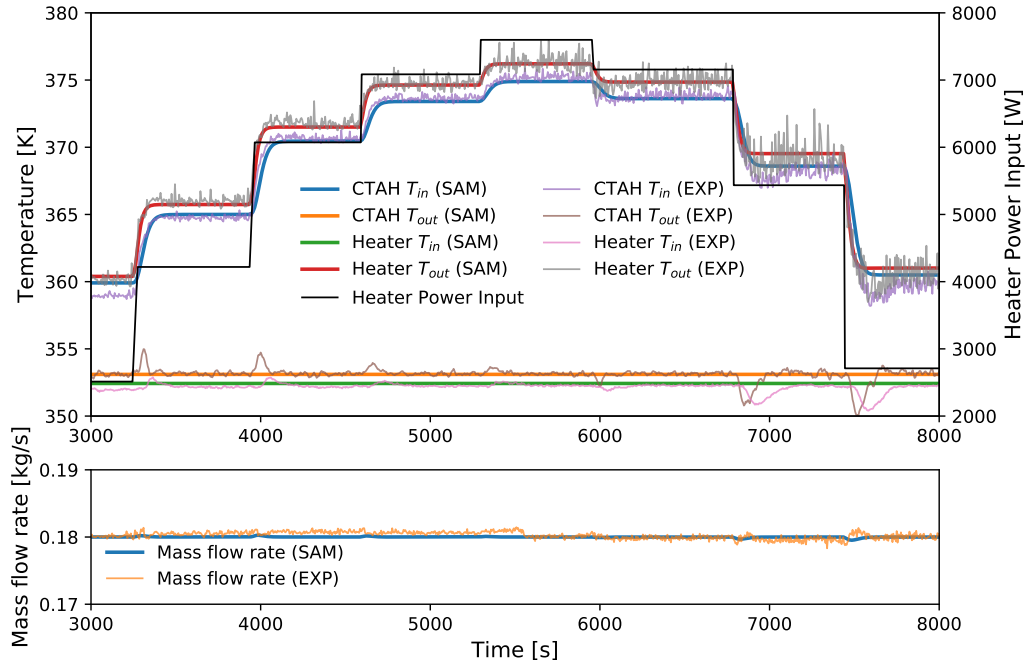


Figure 3.2: Power step change experiments, SAM simulation results compared with CIET experimental data. (SAM)=SAM simulation, (EXP)=Experiment.

3.3 DRACS/DHX Natural Circulation Tests

As key components of the CIET experiments, natural circulation tests were performed to prove the passive decay heat removal concept in the Mk1 PB-FHR design. With heat applied to the heater, natural circulations are to be established in both the primary loop and the DRACS loop. In these experiments, for simplicity purpose, the pump/CTAH loop section along with the bypass flow branch were valved off from the primary loop, which now only consists of the heater-DHX branch. As natural circulations are established, the heat added to the heater is balanced with the heat loss from the primary loop to the DRACS loop via the DRACS heat exchanger (DHX), a tube-in-shell heat exchanger. The heat added to the DRACS loop is eventually lost to the ultimate heat sink, i.e., ambient, via TCHX, which is a fan-cooled oil-to-air heat exchanger.

As discussed earlier in this section, parasitic heat loss is quite significant in some of the CIET tests. This has been observed in most of CIET natural circulation tests. For example, in the selected natural circulation test case A-1, only 54.7% of total electric power ends up to lose in the TCHX (820.7 W heat loss in TCHX vs. 1499.9 W of added electric power). A significant amount of heat is lost as parasitic heat loss, which exhibits to be location dependent. It is thus a challenging task to model the coupled natural circulation loop

without knowing its parasitic heat loss characteristics beforehand. To address this challenge, we follow a two-step approach, similar to what has been done with RELAP5-3D validation (Zweibaum, 2015). For step one, it is focused on the verification/validation of natural circulation in an isolated DRACS loop. As a simple single-loop natural circulation, an analytical solution is first developed to verify code solutions; and validation was performed to consider parasitic heat losses. Following that, a second step validation is performed on the coupled DRACS-DHX natural circulations.

3.3.1 Isolated DRACS natural circulation test

As the first step, SAM code validation is performed on natural circulation in an ‘artificially’ isolated DRACS loop, as shown in Figure 3.3. The heat transferred from the primary loop side to the DRACS loop side in the DHX is modeled as volumetric heat source in the heat structure, which represents DHX tube walls. The amount of heat transferred, Q in Figure 3.3, is back calculated from experimentally measured temperature elevation in DHX tubes for each test case.

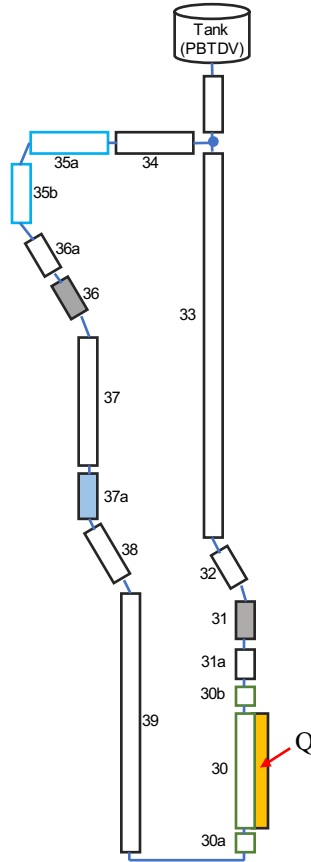


Figure 3.3: SAM input model for the isolated DRACS loop.

3.3.1.1 Solution verification

As a highly simplified case, analytical solutions could be derived for the isolated DRACS natural circulation test case which provides a good opportunity to verify numerical solutions from the SAM code. In the

Table 3.2: Heat addition in the DHX tube walls for isolated DRACS natural circulation simulations, q'''_{wall} is equivalent volumetric heat source

Case	Heat addition [W]	q'''_{wall} [W/m ³]
A-1	931.8	2.314357×10^6
A-2	1088.3	2.703036×10^6
A-3	1338.4	3.324328×10^6
A-4	1470.6	3.652720×10^6
A-5	1699.9	4.222143×10^6
A-6	1876.5	4.660920×10^6
A-7	2137.0	5.307794×10^6
B-1	454.4	1.128688×10^6
B-2	766.2	1.903039×10^6
B-3	1004.4	2.494600×10^6
B-4	1211.2	3.008277×10^6
B-5	1409.0	3.499644×10^6
B-6	1607.4	3.992517×10^6
B-7	1804.6	4.482310×10^6
B-8	2004.9	4.979609×10^6
B-9	2211.0	5.491735×10^6
C-1	582.6	1.447065×10^6
C-2	785.9	1.951969×10^6
C-3	971.4	2.412831×10^6
C-4	1185.2	2.943654×10^6
C-5	1369.1	3.400627×10^6
C-6	1584.1	3.934454×10^6
C-7	1763.7	4.380556×10^6
C-8	1970.0	4.893149×10^6
C-9	2177.0	5.407289×10^6

past, numerical verification of SAM has been done for relatively simpler cases (Hu, 2018). Rigorous numerical verification of system analysis codes in simulations of natural circulation loops is generally difficult, largely due to analytical solutions to such non-linear systems often being unavailable. Only for highly ideal situations, such as the Welander oscillatory instability problem (Welander, 1967), analytical solutions are available, and therefore provided as the reference solution for numerical verification, see for example (Zou et al., 2017). Occasionally, numerical verification was performed in the form of mesh refinement study, using the very-fine mesh numerical results as the reference solution, e.g., (Zhao et al., 2015).

For CIET natural circulation loop, analytical solutions were provided in (Scarlat, 2012). These analytical solutions were later compared with CIET experimental data (Zweibaum, 2015), where quite significant difference between them were observed. There are two major factors responsible for such significant difference: 1) cold-hot legs averaged quantities were used in the analytical solutions (Scarlat, 2012), which introduces extra amount of error; and 2) parasite heat loss in CIET experiments are not insignificant, which is not addressed in such analytical solutions.

For solution verification purpose, an ‘analytical’ solution is derived, which is presented in Appendix C. This solution is obtained for the DRACS loop with further simplification that parasitic heat loss is not considered, which is of course not true in CIET experiments, however, can be simply modeled with SAM. Approximations were also made to derive this solution (see Appendix C), and therefore, the ‘analytical’ solution is not truly analytical. However, it still provides a good reference to gauge the correctness of code implementation (e.g., friction loss coefficient), as well as to identify potential input errors (e.g., form loss co-

efficient and pipe hydraulics diameter). These are all important elements of solution verification for scientific computing (Oberkampf and Roy, 2010). Table 3.3 summarizes SAM solution verification against analytical solutions. SAM predicted natural circulation flow rates are fairly close to those predicted analytically. Based on the results of this solution verification process and existing numerical verification of SAM (Hu, 2018), it has been demonstrated that SAM is well suitable and verified for further validation tasks.

Table 3.3: Solution verification: SAM-predicted results vs. ‘analytical’ solutions for the simplified DRACS natural circulation. SAM=SAM-predicted results; ANA=analytical solution.

Case	\dot{m} : analytical solution [kg/s]	\dot{m} : SAM results [kg/s]	Error= $\frac{SAM-ANA}{ANA}$
A-1	3.4967×10^{-2}	3.5019×10^{-2}	0.15%
A-2	3.7214×10^{-2}	3.7275×10^{-2}	0.16%
A-3	4.0525×10^{-2}	4.0598×10^{-2}	0.18%
A-4	4.2045×10^{-2}	4.2127×10^{-2}	0.20%
A-5	4.4583×10^{-2}	4.4674×10^{-2}	0.20%
A-6	4.6309×10^{-2}	4.6411×10^{-2}	0.22%
A-7	4.8754×10^{-2}	4.8867×10^{-2}	0.23%
B-1	2.4297×10^{-2}	2.4343×10^{-2}	0.19%
B-2	3.0478×10^{-2}	3.0558×10^{-2}	0.26%
B-3	3.4263×10^{-2}	3.4364×10^{-2}	0.30%
B-4	3.6997×10^{-2}	3.7117×10^{-2}	0.32%
B-5	3.9461×10^{-2}	3.9599×10^{-2}	0.35%
B-6	4.1702×10^{-2}	4.1851×10^{-2}	0.36%
B-7	4.3738×10^{-2}	4.3913×10^{-2}	0.40%
B-8	4.5643×10^{-2}	4.5834×10^{-2}	0.42%
B-9	4.7497×10^{-2}	4.7704×10^{-2}	0.44%
C-1	2.7989×10^{-2}	2.8033×10^{-2}	0.16%
C-2	3.1748×10^{-2}	3.1807×10^{-2}	0.19%
C-3	3.4616×10^{-2}	3.4690×10^{-2}	0.22%
C-4	3.7682×10^{-2}	3.7765×10^{-2}	0.22%
C-5	4.0000×10^{-2}	4.0100×10^{-2}	0.25%
C-6	4.2382×10^{-2}	4.2499×10^{-2}	0.28%
C-7	4.4318×10^{-2}	4.4448×10^{-2}	0.29%
C-8	4.6319×10^{-2}	4.6455×10^{-2}	0.29%
C-9	4.8155×10^{-2}	4.8315×10^{-2}	0.33%

3.3.1.2 Validation against CIET experimental data

The input file (see Figure 3.3) is then modified to include parasitic heat loss for validation purpose. The parasitic heat loss is modeled as heat loss from fluid to ambient as heat conduction through pipe walls. Heat transfer area densities of DRACS pipes have been increased to capture other parasitic heat loss effects. We adopt these increased heat transfer area densities from the RELAP5-3D model (Zweibaum, 2015), and numerical results show good agreement with experiment data in terms of parasitic heat loss. However, SAM-predicted mass flow rates are still consistently larger than experimental data for all simulated cases. This indicates that SAM model either consistently overestimates the buoyancy force or underestimates the frictional loss. After examining SAM’s results, it was found that as the hot oil enters TCHX (from pipe 34 to pipe 35a), the oil temperature almost instantaneously drops to the given value of TCHX outlet temperature, and thus the oil temperature in the vertical section of TCHX, i.e., pipe 35b, is uniformly at such a temperature. In reality, the oil temperature distribution in this vertical section should follow a profile having a hot temperature

at the top and $T_{TCHX,out}$ at the bottom. Although it is difficult to determine what exact profile it would follow, as no experimental data are available and the TCHX geometry is quite complex, it is probably a much better approach to assume a, for example, linear distribution rather than a uniform one at $T_{TCHX,out}$. To facilitate a linear temperature distribution in the vertical section, the DRACS input model is slightly modified: pipe 35b is evenly split into two pipes, 35b-1 at the top and 35b-2 at the bottom. Adiabatic wall boundary conditions are now given to pipe 35a and 35b-1. The resulted temperature distribution, uniformly hot temperature at pipe 35b-1 and $T_{TCHX,out}$ at pipe 35b-2, is effectively the same as a linear distribution, when computing the total gravity force in the vertical section of TCHX. After this modification, SAM results are obtained for all three sets of test case. The comparison between SAM results, RELAP5-3D results (Zweibaum, 2015), and experimental results are shown in Figure 3.4 with three different $T_{TCHX,out}$. On these plots, error bars (uncertainties) are not included for experiment data of DRACS mass flow rate, as they are small and would be invisible on the plots even if they are included. For the total 25 tests, the average error between SAM predicted results and experiments is 0.04%, with a standard deviation of 0.5%. Figure 3.5 also shows the comparison between the two mass flow rates, as most of the relative errors are within 1%.

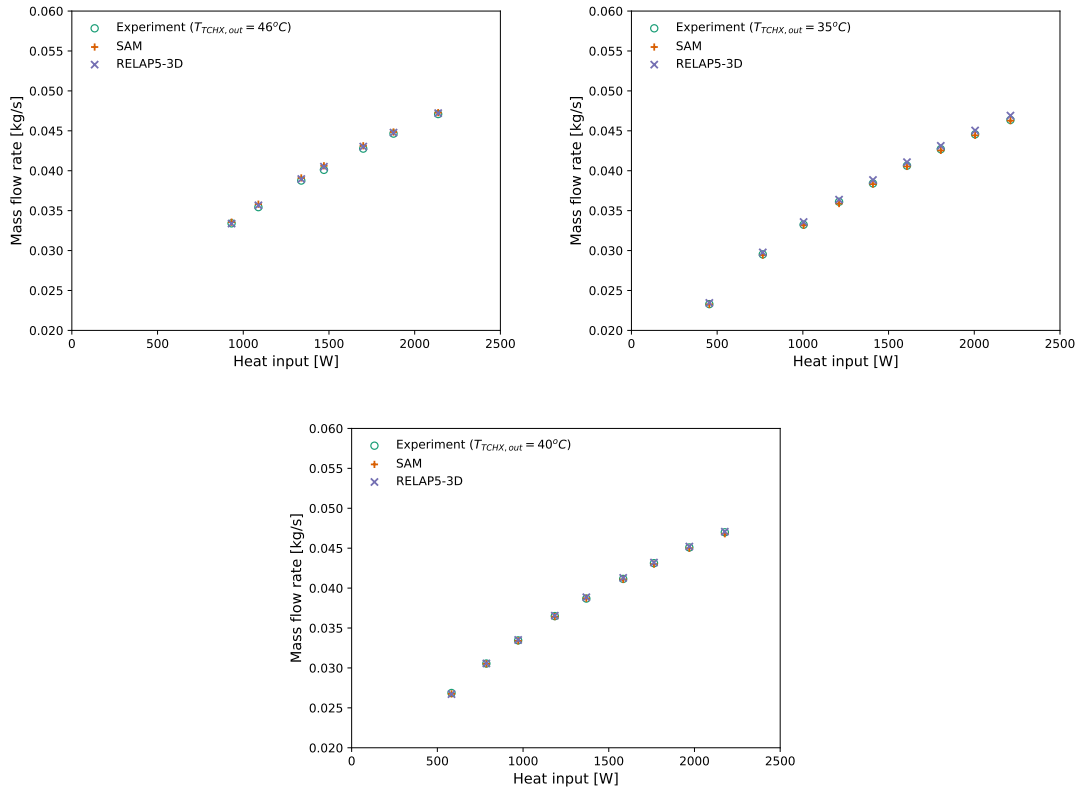


Figure 3.4: Isolated DRACS natural circulation, SAM and RELAP5-3D simulation results compared with CIET experimental data. Top-left: $T_{TCHX,out}=46^{\circ}\text{C}$; Top-right: $T_{TCHX,out}=35^{\circ}\text{C}$; Bottom: $T_{TCHX,out}=40^{\circ}\text{C}$.

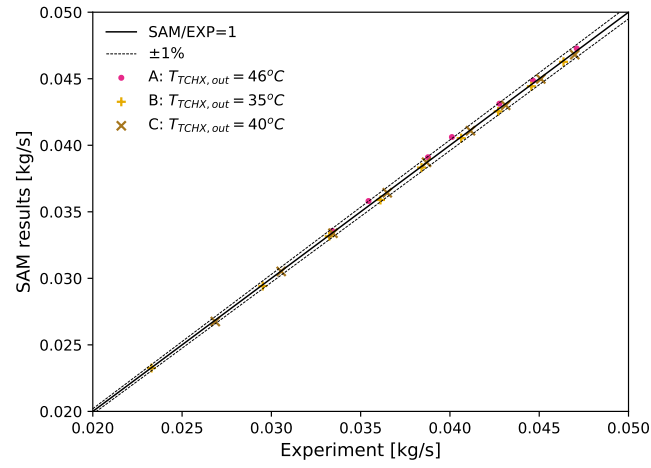


Figure 3.5: Isolated DRACS natural circulation, SAM simulation results compared with CIET experimental data

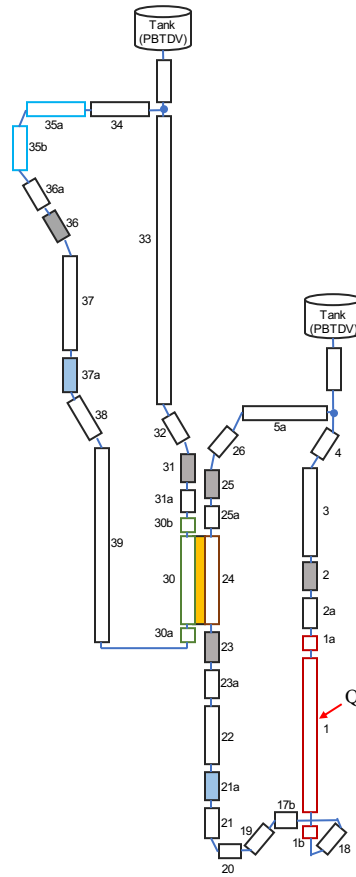


Figure 3.6: SAM input model for coupled DRACS-DHX natural circulations.

3.3.2 Coupled DRACS-DHX natural circulation test

Based on the successful validation against the isolated DRACS natural circulation, we are now ready to perform the validation task of the coupled DRACS-DHX natural circulation test, which is a true representation of the original CIET experiments. The SAM input model includes both the DRACS loop and the heater-DHX loop, as shown in Figure 3.6.

Similar to the isolated DRACS case, the total electric power is not applied to the heater section as input condition; instead, heat addition to the oil is back calculated from its temperature elevation measured from experiments. They are added to the outer wall of the heater pipe in terms of volumetric heat sources, which are listed in Table 3.4 for all cases.

Table 3.4: Heat addition in the heater outer walls for coupled DRACS-DHX natural circulation simulations, q'''_{wall} is equivalent volumetric heat source

Case	Heat addition [W]	q'''_{wall} [W/m ³]
A-1	1479.9	3.749046×10^6
A-2	1653.9	4.189950×10^6
A-3	2014.5	5.103503×10^6
A-4	2178.5	5.518924×10^6
A-5	2395.9	6.069713×10^6
A-6	2491.9	6.312835×10^6
A-7	2696.2	6.830582×10^6
B-1	655.2	1.659765×10^6
B-2	1054.3	2.670992×10^6
B-3	1394.7	3.533297×10^6
B-4	1685.6	4.270303×10^6
B-5	1987.8	5.035710×10^6
B-6	2282.0	5.781189×10^6
B-7	2546.6	6.451475×10^6
B-8	2874.0	7.280983×10^6
B-9	3031.2	7.679058×10^6
C-1	841.0	2.130613×10^6
C-2	1158.7	2.935381×10^6
C-3	1409.2	3.570084×10^6
C-4	1736.1	4.398205×10^6
C-5	2026.3	5.133333×10^6
C-6	2288.8	5.798467×10^6
C-7	2508.7	6.355497×10^6
C-8	2685.8	6.804212×10^6
C-9	2764.5	7.003571×10^6

Parasitic heat loss along the heater-DHX pipes DHX outer shell wall are also calibrated to allow for correct amount of heat loss to the ambient. In DHX, with the default heat transfer coefficient, it has been found that the predicted oil temperature is too high compared to experiment observations. This indicates the default heat transfer coefficient underestimates the shell-to-tube heat transfer in DHX, and has been effectively corrected by increasing the heat transfer area density in both the shell side and tube side of the DHX tubes¹. The calibration process has been performed for only once, and the calibrated heat transfer

¹In (Zweibaum, 2015), page 41, it was reported that this heat transfer coefficient overestimates such heat transfer, while in its RELAP5-3D model, increased heat transfer area densities were actually used, which contradicts the statement. We believe that 'overestimates' could be a typo for 'underestimate'.

coefficients are used for all 25 test cases.

For the coupled natural circulation test cases, comparisons between SAM predicted results, RELAP5-3D results (Zweibaum, 2015), and experimental data are shown in Figure 3.7 for three different $T_{TCHX,out}$. Again, error bars for DRACS mass flow rate are not included. One can also observe that the uncertainties to the measured heater-DHX loop mass flow rate are quite large from these plots. Nevertheless, for all test cases, SAM predicted results on natural circulation mass flow rates in both loop agree with experiment data pretty well. For almost all cases, SAM model does a better job than the RELAP5-3D model. For DRACS loop, the average error between SAM predicted results and experiments is 0.42%, with a standard deviation of 2.54%. For heater-DHX loop, the average error between SAM predicted results and experiments is 1.20%, with a standard deviation of 2.79%.

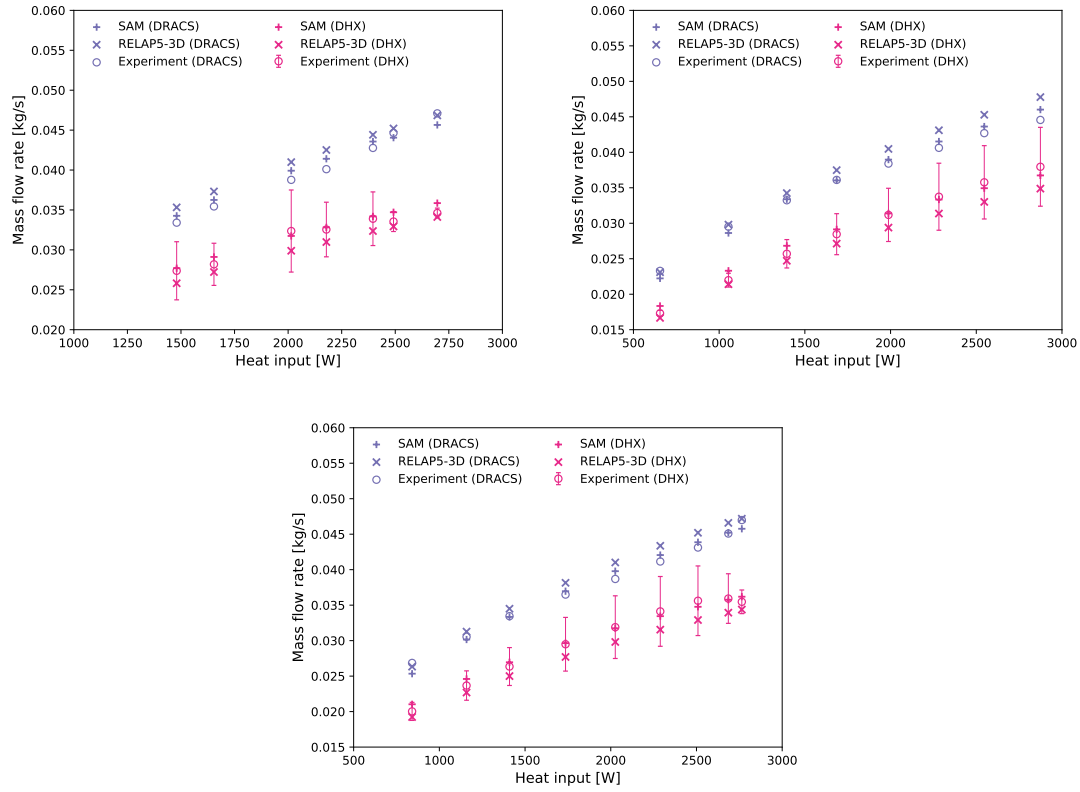


Figure 3.7: Coupled DRACS-DHX natural circulation, SAM and RELAP5-3D simulation results compared with CIET experimental data. Top-left: $T_{TCHX,out}=46^{\circ}\text{C}$; Top-right: $T_{TCHX,out}=35^{\circ}\text{C}$; Bottom: $T_{TCHX,out}=40^{\circ}\text{C}$.

3.3.3 Frequency domain test

Frequency domain tests concern the frequency response of an output signal by examining the relationship between an input and the corresponding output in the variable of interest (Poresky et al., 2017). Frequency domain tests have been adopted in the early molten-salt reactor (MSR) experiments to study the stability and control of such reactor concepts, and since FHRs have similar thermal inertia of fluid and structural materials to MSRs, it is believed that frequency domain tests are also valuable to FHRs concepts (Poresky et al., 2017). The CIET frequency domain tests are rather simple, with heater power being the input signal of simple sinusoidal shape, and heater outlet oil temperature and surface temperature as output signals. The validation

results presented in this section are only preliminary, and more details and analysis will be documented in a separate report.

The CIET frequency domain tests were performed with a new heater model meant to increase the flow area and decrease the heater's surface temperature. This new heater is made up of the same outer tube, a perforated inner tube (with 23% or 51% openings), and a twisted tape inside the inner tube to enhance heat transfer. With SAM, the new heater was modeled with a PBPipe representing the outer tube, and a PBCoupledHeatStructure plate inside the pipe at the tape's dimensions. Currently, the inner perforated tube was not represented by a component. Its presence was however included in the calculations of the flow area and hydraulic diameter. The input model only includes the heater section, with a constant mass flow input (0.18kg/s), and a constant outlet pressure (10^5 Pa). The inlet temperature was not constant but instead followed the inlet temperature from the experiment which fluctuates (with a certain phase lag) at the same frequency that the outlet temperature. The results examine the outlet temperatures of the fluid as well as the surface temperature of the outer-tube's end. A sine power input $P(t) = 9000 + 1000\sin(2\pi ft)$ in Watts, with f the frequency, was applied to the system's outer wall, corresponding to the experiment's power output. The CIET experiment concerns the behavior of output signals, such as its phase delay and amplitudes with different input signal frequencies. Nine frequencies were chosen for this SAM code validation effort:

Table 3.5: Frequencies used in SAM validation

Frequency (Hz)	Period (s)
6.0×10^{-5}	16667 = 4.7h
1.6×10^{-4}	6250 = 1.7h
6.0×10^{-4}	1667 = 27min
1.6×10^{-3}	625
3.2×10^{-3}	312.5
6.0×10^{-3}	166.7
1.6×10^{-2}	62.5
3.2×10^{-2}	31.3
6.0×10^{-2}	16.7

For an example with input power frequency of 6×10^{-3} Hz, the comparisons between SAM results and experimental data are shown in figure 3.8 for fluid temperature at heater outlet, and figure 3.9 for wall surface temperature at heater outlet, respectively. Overall the results from SAM were very similar to the ones in the CIET experiment, both in terms of temperature magnitude and phase shift compared to the input signal. However, SAM predicts a higher average temperatures than those observed in experiment, which can be due to the fact that heat loss is not considered in SAM simulations.

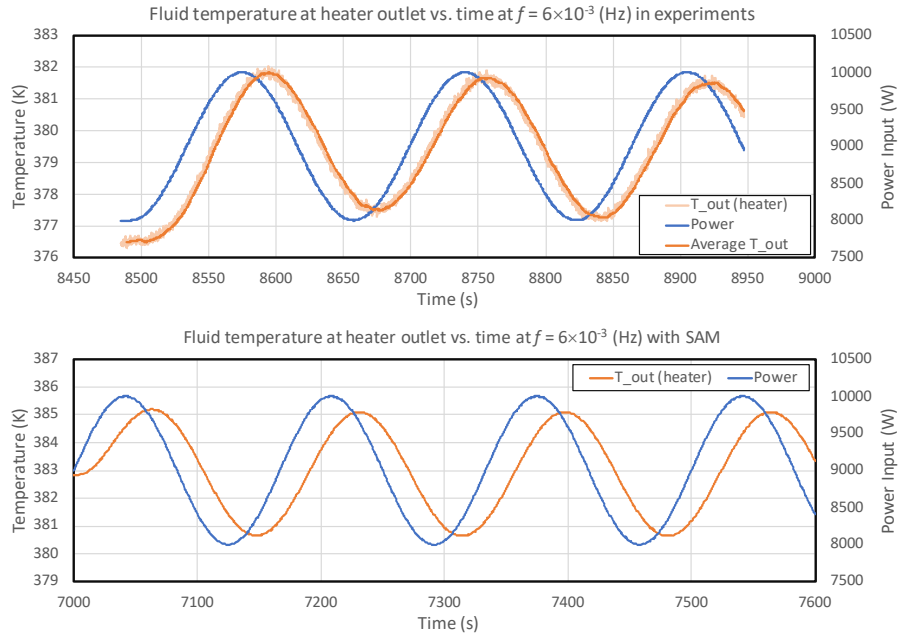


Figure 3.8: Comparison between SAM predicted results (bottom) and experimental data (top) for fluid temperature at heater outlet, with input power frequency at 6×10^{-3} Hz.

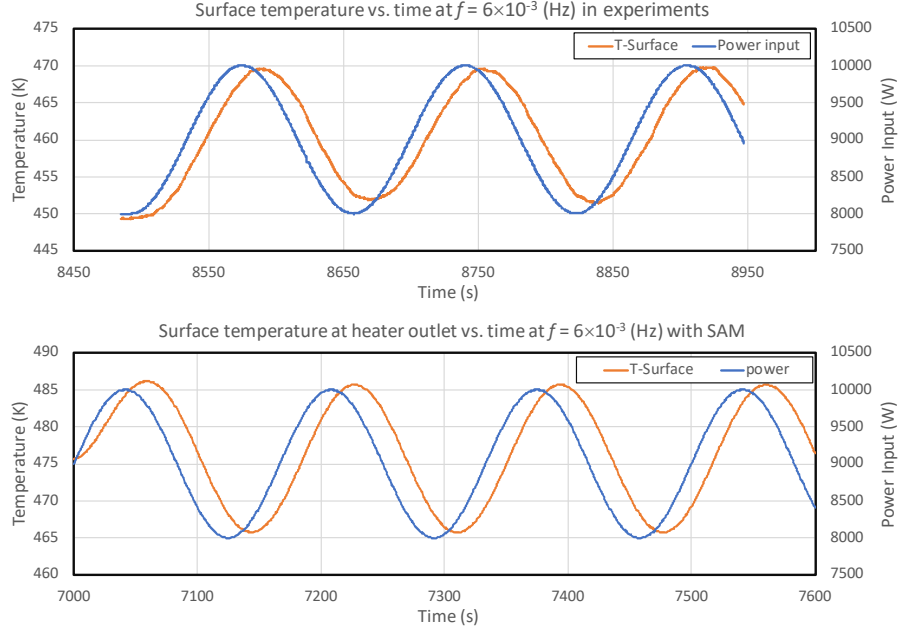


Figure 3.9: Comparison between SAM predicted results (bottom) and experimental data (top) for wall surface temperature at heater outlet, with input power frequency at 6×10^{-3} Hz.

Figures 3.10 and 3.11 summarize the phase shift and heater outlet temperature amplitudes for all nine test cases. The phase shift is quantified as the ratio of time delay to the period of input power in terms of

percentage. For all nine frequencies, SAM predicted results are well aligned with experimental data. Similar to experiment observation, as the frequency increased we could observe both an increase of the phase shift and a decrease of the amplitude. The difference between SAM results and experiment data are relatively larger for the two cases with highest frequencies. It is to be noted that the experiment output signal fluctuates significantly around an average sine value and therefore the uncertainties are larger in determination of both amplitude and phase shift.

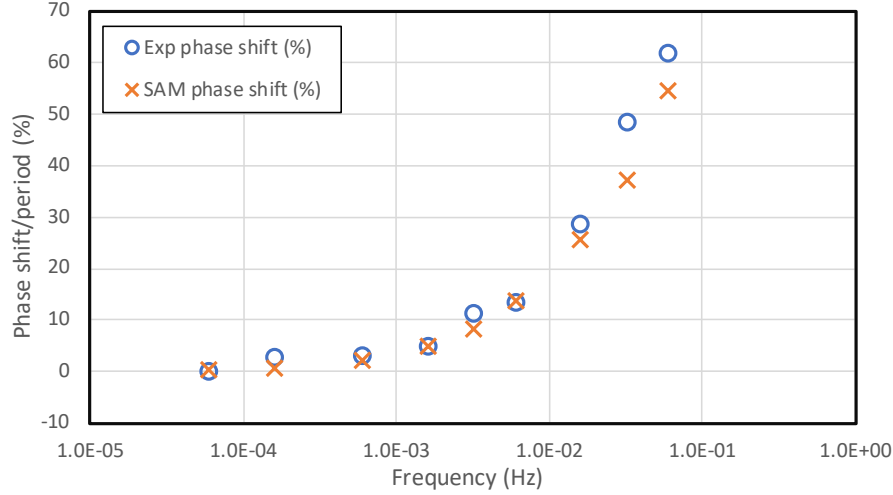


Figure 3.10: SAM predicted phase shift, heater outlet temperature compared to input power, for different input power frequencies.

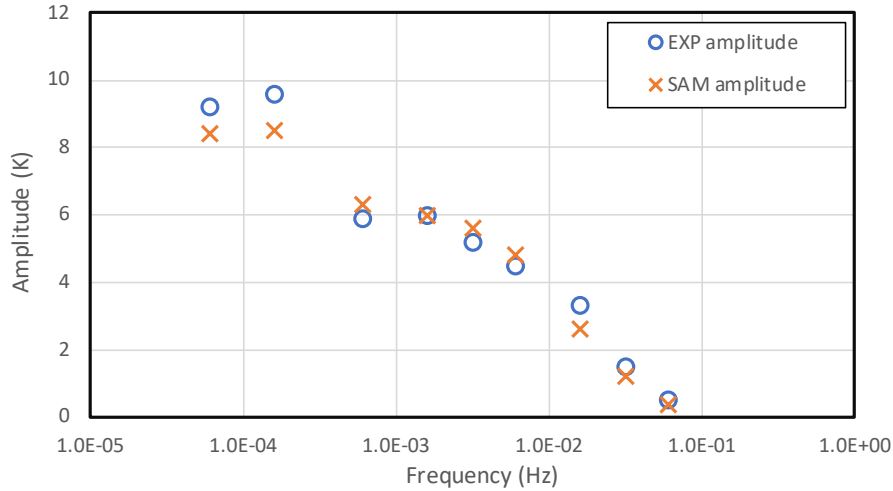


Figure 3.11: SAM predicted heater outlet temperature amplitudes compared with experimental data for different input power frequencies.

The results presented in this section only represents a preliminary validation effort, which is in parallel with another ongoing activity to investigate the frequency response in a more analytical perspective. Here, a brief discussion is provided. In terms of frequency response, clearly, there are at least three time scales come into play, including the obvious one: input signal with $t_{power} = 1/f$.

The second one is also quite obvious, which is the fluid resident time in the heater, $t_{resident} = L/u$, with L being the length of heater and u the fluid velocity.

The third one is associated with the conjugate heat transfer. In a simplified lumped parameter analysis, the wall average temperature can be computed as

$$\frac{T - T_{\infty}}{T_0 - T_{\infty}} = e^{-\text{BiFo}} \quad (3.1)$$

such that the time scale is determined by the product of two non-dimensional numbers, the Biot number

$$\text{Bi} = \frac{\delta h}{k}$$

and the Fourier number

$$\text{Fo} = \frac{\alpha t}{\delta^2}$$

in which, h is the convective wall heat transfer coefficient, δ heater wall thickness, k heater wall thermal conductivity, and α heater wall thermal diffusivity. This third time scale, t_{CHT} , could be obtained, by letting $\text{BiFo} = 1$ (or $\ln 2$), as

$$t_{CHT} = \frac{\rho c_p \delta}{h}$$

However, in this simplified analysis, the fluid temperature, T_{∞} , is assumed to be constant. The deviation of fluid temperature from a constant value, i.e., its amplitude, is simultaneously dependent on many factors, such as fluid thermal physical properties and mass flow rate. As can be seen from discussions above, the frequency response is indeed a complex phenomenon that involves at least three time scales (most likely more than three considering fluid temperature not being constant) and depends on many factors. In CIET experiments, it is almost impossible to investigate the multi-dimensional effects of these wide-spreading parameters for time and cost reasons. Fortunately, SAM code provides a framework to perform these impossible real-life experiments in a numerical way. The results of this ongoing parallel study will be documented in a separate report.

4 Conclusions and Discussions

In this study, the reactor safety analysis code, SAM, is calibrated-validated against three sets of CIET experiments of distinctive characteristics. Selected CIET experiments include: 1) transient heat transfer tests with power step changes under forced-convection conditions; 2) natural circulation tests in coupled DRACS/DHX loops; and 3) frequency response test in the heater. For all these cases, SAM-predicted results showed very good agreement with CIET experimental data, even though they are of completely distinctive characteristics.

For the power step change transients, under forced-convection conditions, there are multiple power step changes, and following each step change, the power maintained at the same level for a long period of time to allow the system reestablish stable conditions. SAM simulations are able to give very good predictions on coolant temperatures for both transient condition that follows each power step change, and quasi-steady state condition when stable condition was reestablished in the flow loop. For natural circulation tests, without pump, natural circulations were established in both the DRACS and DHX loops, such that heat is eventually transferred to from heater to DHX, and eventually to TCHX and is rejected to the ambient. For this experiment validation, a two-step approach was used, the first step for an isolated DRACS loop, and the second step for the coupled DRACS/DHX loop. Numerical verification of SAM code calculation was first performed for an isolated and simplified DRACS natural circulation loop, which is followed by validation in this loop considering heat loss. With a fixed DRACS loop, code validation was then performed for the coupled DRACS/DHX natural circulation tests. SAM simulations were able to predict natural circulation mass flow rates and coolant temperatures in the loop with good agreement to experimental measurements. The frequency

response test concerns the phase shift between the input (power) and output signals (heater outlet coolant and surface temperatures), as well as the amplitude of output signals. For all selected frequency response tests, SAM-predicted results showed very good consistence with experimental observation for both phase shift and outlet temperature magnitudes. Overall, in this study, we have successfully validated the reactor safety analysis code, SAM, against three sets of CIET experiments of distinctive characteristics. This demonstrates that the computer code is suitable for FHRs analysis applications.

The largest uncertainty of both experiment and simulation come from the heat transfer, including both parasitic heat loss from pipes to ambient, and shell-to-tube heat transfer in DHX. Heat transfer coefficients had to be increased in order to capture these effects. For parasitic heat loss, it is most likely due to additional losses through metallic components protruding from the thermal insulation. This, however, does not explain the underestimated heat transfer in DHX. It seems that there is a large uncertainty associated with laminar flow heat transfer using fluids with large Prandtl number. A further investigation into this topic would be necessary to support advanced reactor designs that uses non-traditional coolants, such as molten salts.

In addition to the three sets of experiments used in this validation study, there are more experiment sets and data available from CIET experiments. This includes, for example, loss-of-forced-convection test not yet covered in this study. There are also additional experimental data for natural circulation tests, which includes transient effects due to power change and can be used for further validation of the SAM code.

ACKNOWLEDGEMENTS

This work is supported by U.S. DOE Office of Nuclear Energy's Nuclear Energy Advanced Modeling and Simulation (NEAMS) program. The submitted manuscript has been created by UChicago Argonne, LLC, Operator of Argonne National Laboratory ("Argonne"). Argonne, a U.S. Department of Energy Office of Science laboratory, is operated under Contract No. DE-AC02-06CH11357. The authors would also greatly appreciate support provided by Dr. Per F. Peterson, Dan de Wet, and other students at University of California, Berkeley, for providing experimental data and discussions on this validation effort.

REFERENCES

- C. Andreades, A.T. Cisneros, J.K. Choi, Y.K. Chong, M. Fratoni, S. Hong, L.R. Huddar, K.D. Huff, D.L. Krumwiede, M.R. Laufer, M. Munk, R.O. Scarlat, N. Zweibaum, E. Greenspan, and P.F. Peterson. Technical Description of the “Mark 1” Pebble-Bed Fluoride-Salt-Cooled High-Temperature Reactor (PB-FHR) Power Plant. Technical Report UCBTH-14-002, University of California, Berkeley, 2014.
- C. Andreades, A.T. Cisneros, J.K. Choi, Y.K. Chong, M. Fratoni, S. Hong, L.R. Huddar, K.D. Huff, J. Kendrick, D.L. Krumwiede, M.R. Laufer, M. Munk, R.O. Scarlat, N. Zweibaum, E. Greenspan, , X. Wang, and P.F. Peterson. Design Summary of the Mark-I Pebble-Bed, Fluoride Salt–Cooled, High-Temperature Reactor Commercial Power Plant. *Nuclear Technology*, 195:223–238, 2016.
- J.E. Bickel, N. Zweibaum, and P. F. Peterson. Design, Fabrication and Startup Testing in the Compact Integral Effects Test (CIET 1.0) Facility in Support of Fluoride-Salt-Cooled, High-Temperature Reactor Technology. Technical Report UCBTH-14-009, University of California, Berkeley, 2014.
- R. Hu. SAM Theory Manual. Technical Report ANL/NE-17/4, Argonne National Laboratory, 2017.
- R. Hu. Preliminary SAM Assessment. Technical Report ANL/NE-18/8, Argonne National Laboratory, 2018.
- EG&G Idaho Inc. RELAP5/MOD3 Code Manual, Volume III: Developmental Assessment Problems. Technical Report NUREG/CR-5535, EGG-2596, U.S. NRC, 1990.
- R.L. Moore. Implementation of DOWTHERM A Properties into RELAP5-3D/ATHENA. Technical Report INL/EXT-10-18651, Idaho National Laboratory, 2010.
- W. L. Oberkampf and C. J. Roy. *Verification and Validation in Scientific Computing*. Cambridge, 2010.
- C. Poresky, J.C. Kendrick, and Per F. Peterson. Preliminary Experimental Results for Frequency Response Testing in FHRs and MSRs using the Compact Integral Effects Test. In *Proceedings of 17th International Topical Meeting on Nuclear Reactor Thermal Hydraulics (NURETH 17)*, 2017.
- R. O. Scarlat. *Design of Complex Systems to Achieve Passive Safety : Natural Circulation Cooling of Liquid Salt Pebble Bed Reactors*. PhD dissertation, University of California, Berkeley, 2012.
- R. Upadhy. Instrumentation and Controls Development for the Compact Integral Effects Test Facility. Technical Report UCBTH-15-006, Revision 2, University of California, Berkeley, 2015.
- U.S.NRC. TRACE V5.0 Assessment Manual. Technical Report ML120060208, U.S. NRC, 2008.
- U.S.NRC. NRC Non-Light Water Reactor (Non-LWR) Vision and Strategy, Volume 1 – Computer Code Suite for Non-LWR Design Basis Event Analysis. Technical report, U.S. NRC, 2019.
- P. Welander. On the oscillatory instability of a differentially heated fluid loop. *J. Fluid Mech.*, 29:17–30, 1967.
- H. Zhao, L. Zou, H. Zhang, and R. Martineau. Numerical Verification of RELAP-7 Model For A Single Phase Natural Circulation Loop. *Transactions of the American Nuclear Society*, 112:961–964, 2015.
- L. Zou, H. Zhao, and S. J. Kim. Numerical study on the Welander oscillatory natural circulation problem using high-order numerical methods. *Progress in Nuclear Energy*, 94:162–172, 2017.
- N. Zweibaum. *Experimental Validation of Passive Safety System Models: Application to Design and Optimization of Fluoride-Salt-Cooled, High-Temperature Reactors*. PhD dissertation, University of California, Berkeley, 2015.
- N. Zweibaum, Z. Guo, J. C. Kendrick, and P. F. Peterson. Design of the Compact Integral Effects Test Facility and Validation of Best-Estimate Models for Fluoride Salt–Cooled High-Temperature Reactors. *Nuclear Technology*, 196:641–660, 2016.

Appendices

A CIET Input Model

Table A.1 lists the SAM pipe components of the CIET test facility, as also shown in figure 3.1. In the SAM input model, all components are arranged on the x-z plane ($y=0$), and therefore each pipe's location is determined by its original point (x_0, z_0), its length, and orientation (dx, dz).

The dimensions of the pipe components are listed as follows:

1" nominal schedule 10 304L stainless steel pipe:

- O.D. = 0.033401 m (1.315 inch);
- I.D. = 0.0278638 m (1.097 inch);
- Wall thickness = 0.0027686 m (0.109 inch);
- $D_h = \text{I.D.}$;
- Flow area = $6.097763 \times 10^{-4} \text{ m}^2$;

Heater pipe:

- Outer pipe I.D. = 0.038354 m (1.51 inch)²;
- Outer pipe wall thickness = 0.001905 m (0.075 inch) (based on RELAP5-3D input model (Zweibaum, 2015));
- Inner pipe O.D. = 0.03175 m (1.25 inch);
- Inner pipe wall thickness = 0.0026 m (based on RELAP5-3D input model (Zweibaum, 2015));
- $D_h = 6.604 \times 10^{-3} \text{ m}$;
- Flow area = $3.636133 \times 10^{-4} \text{ m}^2$;

DHX tubes:

- Number of pipes = 19;
- I.D. = 0.00635 m;
- O.D. = 0.00794 m³;
- Wall thickness = $7.95 \times 10^{-4} \text{ m}$;
- $D_h = \text{I.D.}$;
- Flow area = $6.0172 \times 10^{-4} \text{ m}^2$;

DHX shell side:

- I.D. = 0.0508 m;
- O.D. = 0.0504 m;

²Value of 1.51 inch is based on the RELAP5-3D input model (Zweibaum, 2015), in which the inner radius of outer pipe is $1.92 \times 10^{-2} \text{ m}$. This value is slightly different than the value, 0.0381 m, reported in Table2-5 of (Bickel et al., 2014).

³The values of I.D. and O.D. used in (Zweibaum, 2015) are quite different than those reported in (Bickel et al., 2014), which are used in SAM input model.

- Wall thickness = 0.0016 m;
- $D_h = 6.857144 \times 10^{-3}$ m;
- Flow area = 1.086058×10^{-3} m²;

Heater pipe for frequency response test:

- Outer pipe (Same as the original heater design)
- Inner pipe O.D. = 0.03175 m (1.25 inch);
- Inner pipe wall thickness = 0.0026 m (based on RELAP5-3D input model ([Zweibaum, 2015](#)));
- $D_h = 6.604 \times 10^{-3}$ m;
- Flow area = 3.636133×10^{-4} m²;

The form loss coefficients of the entire loop is shown in Figure [A.1](#). For each static mixer, flowmeter and heat exchanger, its combined form loss and frictional loss coefficient is given as a function of Reynolds number, obtained by fitting pressure drop experimental data ([Zweibaum, 2015](#)). This requires that the frictional coefficients of these components are manually set to zero, to avoid double accounting their frictional pressure loss. For mixers and flowmeters, schedule 10 pipe dimensions are used such that correct Reynolds number (with respect to the fitted correlations) could be calculated, as their combined form loss and friction loss coefficients were fitted using schedule 10 pipe diameters.

Table A.1: Pipe components of SAM input model for the CIET test facility

Index	Description	Length [m]	x0 [m]	z0 [m]	dx [m]	dz [m]	# of elements
1b	heater pipe	0.19685	0	0	0	0.19685	2
1	heater pipe	1.6383	0	0.19685	0	1.6383	15
1a	heater pipe	0.0889	0	1.83515	0	0.0889	2
2a	1" Schedule-10 pipe	0.149425	0	1.92405	0	0.149425	2
2	Mixer	0.33	0	2.073475	0	0.33	2
3	1" Schedule-10 pipe	1.2827	0	2.403475	0	1.2827	12
4	1" Schedule-10 pipe	0.2413	0	3.686175	0.155931	0.18415	2
5a	1" Schedule-10 pipe	0.37465	-0.218719	3.870325	0.37465	0	4
5b	1" Schedule-10 pipe	0.37465	0.155931	3.870325	0.37465	0	5
6a	1" Schedule-10 pipe	0.1526	0.530581	3.870325	0.094941	0.119470	2
6	Mixer	0.33	0.625522	3.989795	0.205311	0.258355	2
7a	CTAH-pipe	0.3302	0.830833	4.24815	0	-0.3302	3
7b	CTAH-pipe	1.2342	0.830833	3.91795	1.2342	0	11
8a	1" Schedule-10 pipe	0.22245	2.065033	3.91795	0	-0.22245	2
8	Mixer	0.33	2.065033	3.6955	0	-0.33	2
9	1" Schedule-10 pipe	0.7112	2.065033	3.3655	0.522401	-0.4826	7
10	1" Schedule-10 pipe	2.4511	2.587433	2.8829	0	-2.4511	22
11	1" Schedule-10 pipe	0.4826	2.587433	0.4318	-0.215526	-0.4318	4
12	1" Schedule-10 pipe	0.333375	2.371907	0	-0.333375	0	3
13	1" Schedule-10 pipe	1.273175	2.038532	0	-1.273175	0	12
14	1" Schedule-10 pipe	0.6687	0.765357	0	0	0.6687	6
14a	Flowmeter	0.36	0.765357	0.6687	0	0.36	2
15	1" Schedule-10 pipe	0.3556	0.765357	1.0287	-0.231557	-0.269875	3
16	1" Schedule-10 pipe	0.644525	0.533800	0.758825	0	-0.644525	6
17a	1" Schedule-10 pipe	0.37846	0.533800	0.1143	-0.37846	0	4
17b	1" Schedule-10 pipe	0.094615	0.155340	0.1143	-0.094615	0	2
18	1" Schedule-10 pipe	0.1778	0.155340	0.1143	-0.136192	-0.1143	2
19	1" Schedule-10 pipe	0.219075	0.0607249	0.1143	-0.186894	-0.1143	2
20	1" Schedule-10 pipe	0.33655	-0.126169	0	-0.33655	0	3
21	1" Schedule-10 pipe	0.487725	-0.462719	0	0	0.487725	5
21a	1" Schedule-10 pipe	0.36	-0.462719	0.487725	0	0.36	2
22	1" Schedule-10 pipe	0.69215	-0.462719	0.847725	0	0.69215	6
23a	1" Schedule-10 pipe	0.0891	-0.462719	1.539875	0	0.0891	2
23	Mixer	0.33	-0.462719	1.628975	0	0.33	2
24	DHX Shell side	1.18745	-0.462719	1.958975	0	1.18745	11
25a	1" Schedule-10 pipe	0.22245	-0.462719	3.146425	0	0.22245	2
25	Mixer	0.33	-0.462719	3.368875	0	0.33	2
26	1" Schedule-10 pipe	0.2159	-0.462719	3.698875	0.131216	0.17145	2
30a	DHX Tube side	0.111125	-0.562719	1.84785	0	0.111125	2
30	DHX Tube side	1.18745	-0.562719	1.958975	0	1.18745	11
30b	DHX Tube side	0.18415	-0.562719	3.146425	0	0.18415	2
31a	1" Schedule-10 pipe	0.143075	-0.562719	3.330575	0	0.143075	2
31	Mixer	0.33	-0.562719	3.47365	0	0.33	2
32	1" Schedule-10 pipe	0.238125	-0.562719	3.80365	-0.138541	0.193675	2
33	1" Schedule-10 pipe	3.0099	-0.701260	3.997325	0	3.0099	28
34	1" Schedule-10 pipe	0.55245	-0.701260	7.007225	-0.55245	0	5
35a	TCHX-pipe	1.148475	-1.253710	7.007225	-1.148475	0	11
35b	TCHX-pipe	0.415925	-2.402185	7.007225	0	-0.415925	4
36a	1" Schedule-10 pipe	0.2034	-2.402185	6.5913	0.104768	-0.174343	2
36	Mixer	0.33	-2.297418	6.416957	0.169976	-0.282857	2
37	1" Schedule-10 pipe	1.7736	-2.127442	6.1341	0	-1.7736	16
37a	Flowmeter	0.36	-2.127442	4.3605	0	-0.36	2
38	1" Schedule-10 pipe	0.33655	-2.127442	4.0005	0.205273	-0.2667	3
39	1" Schedule-10 pipe	1.91135	-1.922169	3.7338	0.310566	-1.88595	18

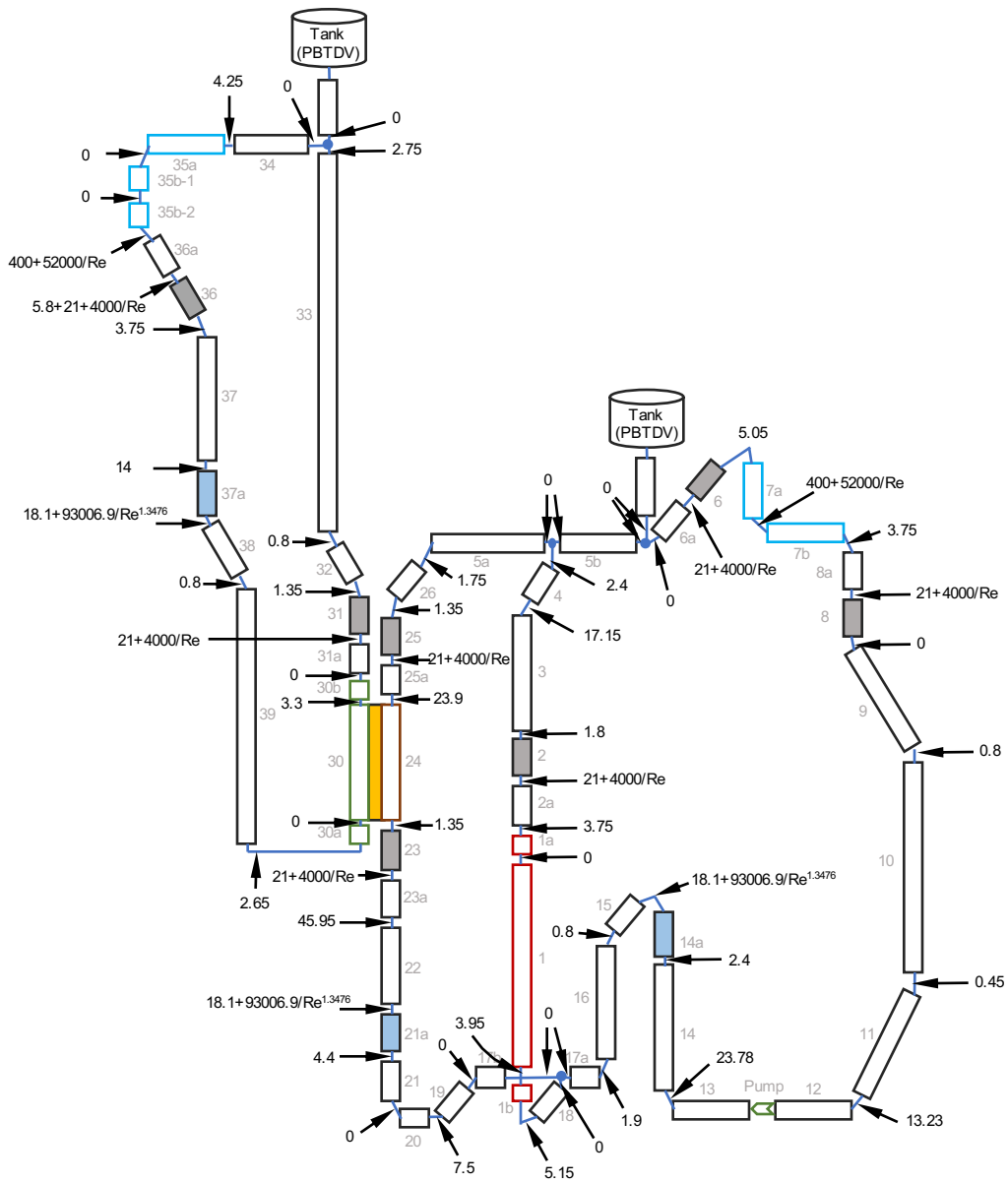


Figure A.1: Form loss coefficients used in the SAM CIET input model

B Material Properties

B.1 304L stainless steel

- Density, $\rho = 8030 \text{ [kg/m}^3\text{]}$;
- Thermal conductivity: Table [B.1](#);
- Heat capacity: Table [B.1](#).

B.2 Copper

- Density, $\rho = 8940 \text{ [kg/m}^3\text{]}$;
- Thermal conductivity: Table [B.2](#);
- Heat capacity: Table [B.2](#).

B.3 Fiberglass

- Density, $\rho = 20 \text{ [kg/m}^3\text{]}$;
- Thermal conductivity: Table [B.3](#);
- Heat capacity, $c_p = 844 \text{ [J/kg}\cdot\text{K]}$.

Table B.1: Temperature-dependent thermal conductivity and heat capacity for 304L stainless steel ([Zweibaum, 2015](#))

Temperature [K]	Thermal conductivity [W/(m·K)]	Heat Capacity [J/(kg·K)]
250.0	14.31	443.3375
300.0	14.94	457.0361
350.0	15.58	469.4894
400.0	16.21	480.6974
450.0	16.85	490.6600
500.0	17.48	500.6227
700.0	20.02	526.7746
1000.0	23.83	551.6812

Table B.2: Temperature-dependent thermal conductivity and heat capacity for copper ([Zweibaum, 2015](#))

Temperature [K]	Thermal conductivity [W/(m·K)]	Heat Capacity [J/(kg·K)]
200.0	-	355.7047
250.0	406	373.6018
300.0	401	384.7875
350.0	396	392.6174
400.0	393	398.2103
500.0	386	407.1588
1000.0	352	417.2260

Table B.3: Temperature-dependent thermal conductivity for fiberglass ([Zweibaum, 2015](#))

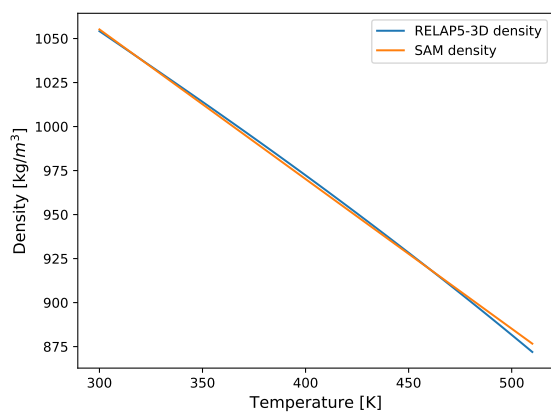
Temperature [K]	Thermal conductivity [W/(m·K)]
250.0	0.028616
293.15	0.033060
350.0	0.038916
400.0	0.044066
500.0	0.054366
600.0	0.064666

B.4 Dowtherm A

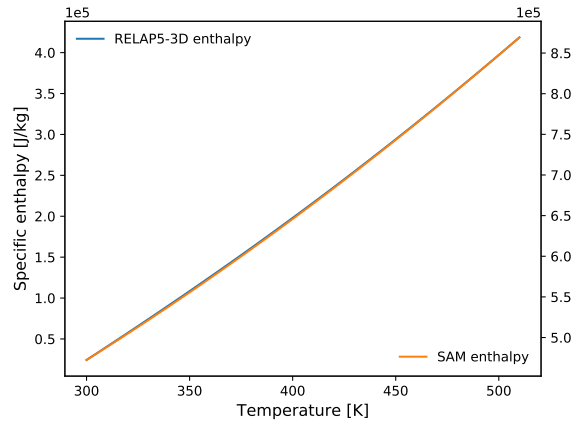
In SAM, thermal physical properties of Dowtherm A are given as functions of its temperature T in °C,

$$\begin{aligned}
 \rho &= 1078 - 0.85T \quad \text{kg/m}^3 \\
 \mu &= \frac{0.130}{T^{1.072}} \quad \text{kg/(m·s)} \\
 c_p &= 1518 + 2.82T \quad \text{J/(kg·K)} \\
 h &= h_0 + 1518(T - T_0) + \frac{2.82}{2}(T^2 - T_0^2) \quad \text{J/kg} \\
 k &= 0.142 - 0.00016T \quad \text{W/(m·K)}
 \end{aligned}$$

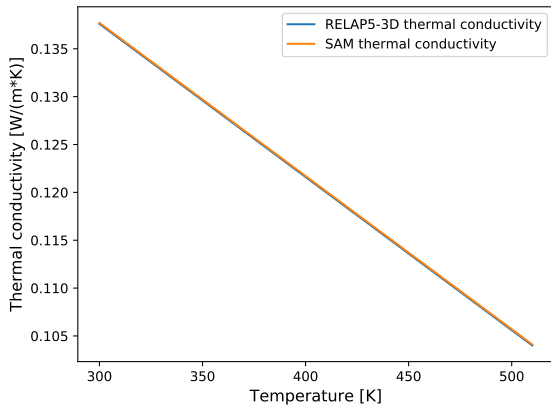
with $T_0 = 20$ °C, and $h_0 = c_p(T_0) \times (T_0 + 273.15)$. It is important to note that Dowtherm A thermal physical properties implemented in the RELAP5-3D code ([Moore, 2010](#)) have different formulations than what are implemented in SAM. Both implementations give similar results, except for viscosity, which shows around 5% difference. There is an offset in the absolute values of specific enthalpy between the two implementations, which is unimportant, since only the relative value matters. These properties are plotted in Figure [B.1](#).



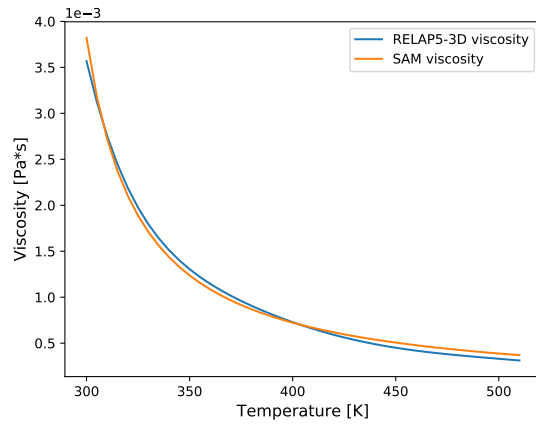
(a) Density



(b) Specific enthalpy



(c) Thermal conductivity



(d) Viscosity

Figure B.1: Dowtherm A thermal physical properties implemented in SAM and RELAP5-3D.

C Analytical Solutions for Isolated DRACS Natural Circulation

The purpose of this section is to derive a more accurate “analytical” solution to the CIET’s DRACS natural circulation loop with zero parasitic heat loss, which will be used to verify the SAM computer code. Fig. C.1 shows a simplified schematic drawing of the isolated DRACS loop with such a simplification, with cold leg to the left and hot leg to the right.

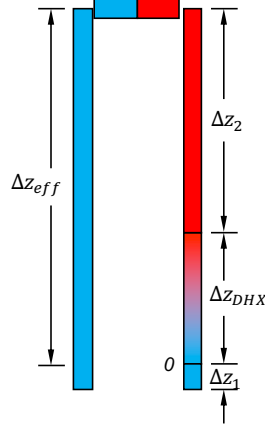


Figure C.1: A simplified schematic drawing of the DRACS loop

The solution to the natural circulation mass flow rate at the steady state can be found by equating the buoyancy force and the frictional loss. The buoyancy force can be calculated by integrating the gravity force between the two legs along the effective height, Δz_{eff} , as shown in Fig. C.1. The temperature and fluid density profiles are shown in Fig. C.2. Assuming the temperature profile, and thus density profile, is linear in the heated section, $[0, \Delta z_{DHX}]$. The buoyancy force is therefore is the shaded area in Fig. C.2 multiplied by the gravity constant,

$$\begin{aligned}\Delta P_B &= \frac{1}{2} (\rho_C - \rho_H) g \Delta z_{DHX} + (\rho_C - \rho_H) g \Delta z_2 \\ &= (\rho_C - \rho_H) g \left(\Delta z_2 + \frac{1}{2} \Delta z_{DHX} \right) \\ &= a g \Delta T \left(\Delta z_2 + \frac{1}{2} \Delta z_{DHX} \right)\end{aligned}\tag{C.1}$$

in which, subscripts ‘C’ and ‘H’ denote cold and hot leg, respective; and ‘B’ denotes ‘buoyancy’. Analytically, the temperature profile in the heated section, $[0, \Delta z_{DHX}]$, is not perfectly linear, and therefore equation (C.1) introduces numerical error in the heated section. Its total effect to the buoyancy force evaluation is rather small, given that the heated section is a small fraction of the total effective height ($\Delta z_{DHX} / \Delta z_{eff} < 0.25$ for CIET), and that the temperature profile is very close to linear when ΔT is reasonably small.

The temperature elevation in the heated section can be found by solving the energy balance equation,

$$\begin{aligned}\frac{Q}{\dot{m}} &= h(T_H) - h(T_C) \\ &= c_{p,C} \Delta T + \frac{b}{2} \Delta T^2.\end{aligned}\tag{C.2}$$

However, note that this is only true for $c_p = a + bT$ (see Appendix B.4). In the equation above, $c_{p,C}$ is c_p at the cold leg temperature; Q is the total heat applied to the heater; and \dot{m} is the natural circulation mass flow

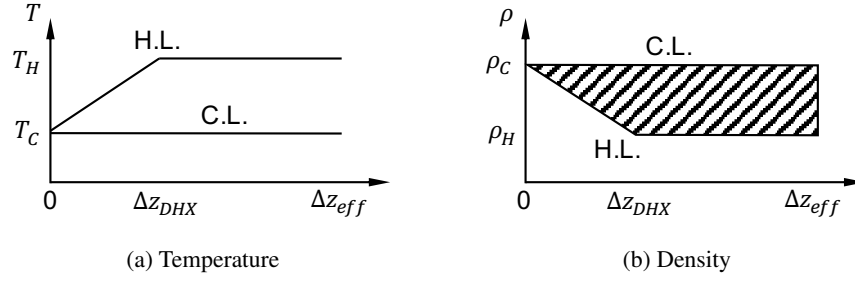


Figure C.2: Temperature and density profiles in the simplified DRACS loop (C.L. = cold leg; H.L. = hot leg).

rate through the heater. The only physically correct solution of ΔT to this quadratic equation is,

$$\Delta T = \frac{-c_{p,C} + \sqrt{c_{p,C}^2 + 2b\frac{Q}{\dot{m}}}}{b} \quad (\text{C.3})$$

Plugging this solution into Equation (C.1), one could obtain the buoyancy force as a non-linear function of mass flow rate, \dot{m} , for any given power, Q . A schematic drawing of fluid temperature and density profiles in the cold and hot legs of the DRACS loop is shown in figure C.2.

On the other hand, the total pressure drop due to friction and form loss is simply the summation of these losses in each pipe section,

$$\Delta P_f = \sum_i \left(K + f \frac{L}{D_h} \right)_i \frac{1}{2} \rho_i u_i^2$$

For flow regimes covered in CIET experiments, only the laminar flow is concerned, and the friction factor is,

$$f = \frac{64}{\text{Re}} = \frac{\dot{m} D_h}{\mu A}$$

Therefore, the total pressure drop ΔP_f is,

$$\Delta P_f = \sum_i \left[\left(K + \frac{\dot{m} L}{\mu A} \right) \frac{\dot{m}^2}{2 \rho A^2} \right]_i \quad (\text{C.4})$$

Whenever μ and ρ is not a constant in a pipe section, averaged values based on inlet and outlet values are used in evaluating the pressure drop, for example, $\bar{\rho} = (\rho_C + \rho_H)/2$ for the heated DHX section. This, again, introduces numerical error in estimation of pressure drop in the DHX section, and only in the DHX section. However, its effect to the total pressure loss the entire DRACS loop is small, as the DHX section only accounts for $\sim 10\%$ of the total pressure drop.

By equating the total pressure drop to the buoyancy force, a non-linear equation is obtained for mass flow rate, \dot{m} , for any given power, Q . Solution to this nonlinear equation could be obtained numerically, for example, a simple bisection method.



Nuclear Science & Engineering Division

Argonne National Laboratory
9700 South Cass Avenue, Bldg. 208
Argonne, IL 60439

www.anl.gov



Argonne National Laboratory is a U.S. Department of Energy
laboratory managed by UChicago Argonne, LLC